Effect of Ship Tilting and Motion on Amine Absorber with Structured-Packing for CO_2 Removal from Natural Gas

Dung Anh Pham and Young-Il Lim
CoSPE, Dept. of Chemical Engineering, Hankyong National University, Jungang-ro 327, Anseong-si, Gyeonggi-do 456-749, Korea

Hyunwoo Jee, Euisub Ahn, and Yongwon Jung
GS E&C, Gran Seoul, 33 Jonro Jongno-gu, Seoul 110-121, Korea

DOI 10.1002/aic.14962
Published online August 1, 2015 in Wiley Online Library (wileyonlinelibrary.com)

A gas-liquid Eulerian porous media computational fluid dynamics (CFD) model was developed for an absorber with structured packing to remove CO_2 from natural gas by mono-ethanol-amine (MEA). The three-dimensional geometry of the amine absorber with Mellapak 500.X was constructed to investigate the effect of the tilting and motion experienced on ships and barges for offshore plants. The momentum equation included porous resistance, gas-liquid momentum exchange, and liquid dispersion to replace structured-packing by porous media. The mass equation involved mass transfer of CO_2 gas into MEA solution, and one chemical reaction. Parameters of the CFD model were adjusted to fit experimental data measured in the CO_2-MEA system. As the tilting angle increased, the liquid holdup and effective interfacial area decreased and CO_2 removal efficiency was lowered. The uniformity of liquid holdup deteriorated by 10% for a 3° static tilting, and a rolling motion with 4.5° amplitude and 12 s period, respectively. © 2015 American Institute of Chemical Engineers *AIChE J*, 61: 4412–4425, 2015

Keywords: natural gas, CO_2 removal, amine absorber, structured-packing, computational fluid dynamics, ship motion

Introduction

The amine absorption technology for the removal of acid gas such as CO_2 and H_2S is well-established with numerous industrial installations[1] and is ready for large scale use.[2] Aqueous solutions of ethanolamine, especially mono-ethanol-amine (MEA), diethanolamine, and methyl diethanolamine, are often used for the absorbent because of low volatility, thermal stability, high reactivity, and low cost.[3,4] The performance of the amine absorber is generally determined by mass-transfer efficiency of column packings providing the gas and liquid contacting area.[5]

Structured packings are well recognized as column internal devices offering excellent mass-transfer efficiency and low pressure drop.[5–8] Structured packing with corrugated and perforated metal sheet is preferably used, when a minimization of pressure drop is important or when columns are subject to motion (offshore applications).[9,10]

Nonstationary platforms such as FPSO (floating production, storage, and offloading) and FLNG (floating liquefied natural gas) are subject to angular and translational motions.[9] In typical motion conditions, there are three angular motions (roll, pitch, and yaw), and three linear motions (surge, sway, and heave).[11] The rolling angular motion results in an offset of the column axis from the vertical line, which is referred to as dynamic tilting. Permanent offset of the column axis from the vertical is called the static tilting, which can be caused by weather conditions or unbalanced product storage.[9]

Liquid and/or gas mal-distribution of the column is one of the main issues in the offshore operation. The ship tilting and motion can induce liquid mal-distribution in the amine absorber.[10,11] Liquid flows along the wall on the tilting side, whereas on the other side of the column a dry area can be formed.[9] Pressure drop may be hardly affected by the gas and liquid mal-distribution.[10]

The effect of gas mal-distribution induced by column internals such as gas and liquid distributors, and liquid collectors was examined using computational fluid dynamics (CFD)[12] in a single phase. Owens et al. (2013) examined gas-phase hydrodynamics by a three-dimensional (3-D) turbulent CFD model, considering a real geometry of a corrugated and perforated structured-packing.[7] The two-fluid porous media CFD model was used for the large-scale amine absorber.[13–15] Fourati et al.[13] addressed a gas-liquid porous media CFD model incorporated with the porous resistance, momentum transfer between the two phases, and liquid dispersion. In Pham et al.,[14] the gas-liquid porous media CFD model was integrated with mass transfer and chemical reaction in an amine absorber with Mellapak 500.X (M500X). However, there is little information available in the public literature related to hydrodynamics and mal-distribution of columns subject to motion.[10]

In this article, particular attention is paid to the liquid mal-distribution encountered in amine absorbers subject to the static tilting and the rolling motion. The gas-liquid porous media CFD model[13,14] is used to investigate the effect of the ship tilting and

Correspondence concerning this article should be addressed to Y.-I. Lim at limyi@hknu.ac.kr.

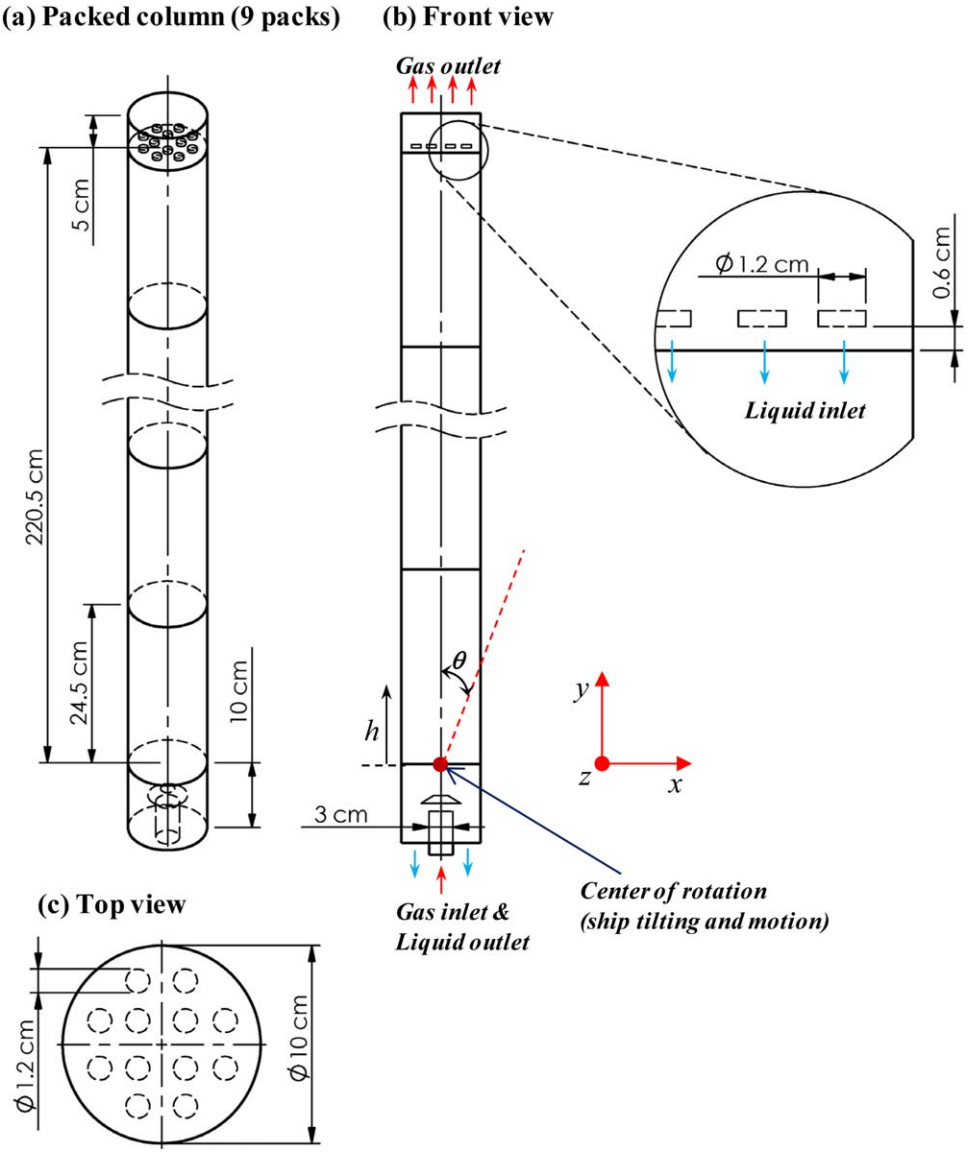

Figure 1. Geometry of amine absorber for CFD calculation domain.

[Color figure can be viewed in the online issue, which is available at wileyonlinelibrary.com.]

motion on pressure drop, liquid holdup, effective interfacial area, liquid mal-distribution, and CO_2 removal efficiency. The tilting angle ranges from 0° to 4.5° and the period of the rolling motion is set to 6 and 12 s. The offshore condition is applied to a hypothetical porous media packing representing M500X.

Amine Absorber with Structured Packing

An amine absorber with nine packs of M500X[5,16] was chosen to examine the effect of ship tilting and motion. Figure 1 illustrates the 3-D geometry of the absorber. One M500X pack has a height of 24.5 cm and a diameter of 10 cm. M500X has a specific surface area (a_s) of 500 m^2/m^3, a corrugated angle of 60°, and a voidage (ε) of 0.91.[16] The corrugated metal sheet with grooves is perforated for facilitating liquid traveling between two sheets and the packs are turned by 90° from each other.[17] As the structured-packing was assumed as a porous medium in this study, the geometric characteristics of the packing were not fully considered.

The column temperature often goes through a maximum near the bottom of the absorption column,[18] because of the heat of absorption and the exothermic reaction in the liquid phase. Some temperature difference between the gas and liquid phases also exists.[16] An increase in temperature results in higher mass transfer and reaction rate. However, the high temperature makes the CO_2 absorption unfavorable in the thermodynamic point of view.[18] In this study, the packing area was modeled as an isothermal porous media zone with porous resistance and liquid dispersion.

The height (h) originates from the bottom of the first pack. The center of rotation is situated at the center of the packing bottom, as shown in Figure 1b. The tilting angle (θ) is measured as a deviation of the column axis from the vertical axis in the x-y plane. The liquid distributor with 12 holes is displayed in the top view in Figure 1c. The MEA solution is injected through the liquid distributor, and natural gas containing 15 mol % CO_2 enters from the bottom of the amine absorber.

Meshing of CFD domain

The mesh structure of the amine absorber is shown in Figure 2. The top of the column has a fine hexahedral mesh structure

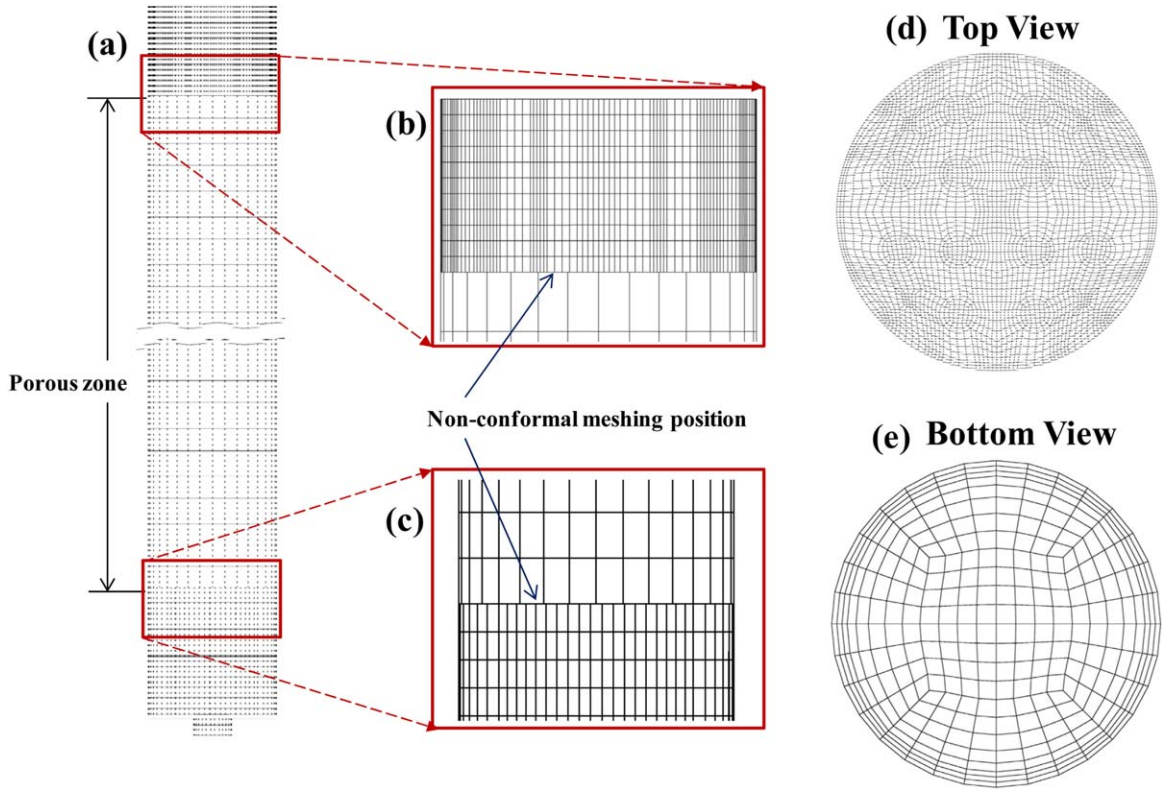

Figure 2. Nonconformal mesh structure in top and bottom of packing zone.

[Color figure can be viewed in the online issue, which is available at wileyonlinelibrary.com.]

to represent the 12 holes in the liquid distributor, while a relatively coarse mesh structure is used in the porous zone (see Figure 2a). The nonconformal meshing strategy is applied to reduce the number of cells at the interface between the gas and liquid distributors and the porous zone (see Figures 2b, c), where the top and bottom views of the interface have the different mesh structure (see Figures 2d, e).

The high-resolution mesh having 36,480 hexahedral cells was built in the nonporous zone (top and bottom of the column) because of the inlet and outlet of gas and liquid. The mesh structure of the nonporous zone was fixed. Coarse, medium, and fine meshes (about 11,900, 37,400, and 103,500, respectively) were built in the porous zone to test the mesh independence.

Tilting and motion

The tilting and motion can cause a serious liquid maldistribution in the offshore amine absorber. The unit position vector, $\left(\vec{u}_d\right)_{\text{tilt}}$, with a static tilting angle (θ) is expressed as

$$\left(\vec{u}_d\right)_{\text{tilt}} = \frac{\vec{r}}{|\vec{r}|} = \sin\theta \cdot \vec{i} + \cos\theta \cdot \vec{j} \tag{1}$$

where $\vec{i}$ and $\vec{j}$ are the direction vectors of x and y axes. Here, y is the vertical axis of the column. $\vec{r}$ is the position vector and $|\vec{r}|$ is the magnitude of $\vec{r}$.

The sliding mesh (or moving mesh) method is used to perform the motion of the amine absorber. Modified governing equations of continuity, momentum, and mass are shown in Table 1. There are two kinds of the velocity vector. One is the fluid velocity such as $\vec{u}_{\text{G}}$ and $\vec{u}_{\text{L}}$ of the gas and liquid phases, respectively, in the stationary reference frame. The other is $\vec{v}_{\text{mesh}}$ is the mesh velocity arising from the ship motion. The mesh velocity ($\vec{v}_{\text{mesh}}$) is defined as the outer product of the angular velocity ($\vec{\omega}=d\theta/dt$) and the position vector ($\vec{r}$) (ANSYS Fluent user's guide, 2015)

$$\vec{v}_{\text{mesh}} = \vec{\omega} \times \vec{r} \tag{2}$$

The unit vector under the rolling motion representing the roll and pitch of the angular motion, $\left(\vec{u}_d\right)_{\text{roll}}$, is

$$\left(\vec{u}_d\right)_{\text{roll}} = \frac{\vec{r}}{|\vec{r}|} = \sin\theta \cdot \vec{i} + \cos\theta \cdot \vec{j}$$
$$\theta = \theta_{\max}\cos\left(\frac{2\pi}{T}t + \frac{\pi}{2}\right) \tag{3}$$

where $\theta_{\max}$ is the amplitude of the angular motion, and T is the period. The two unit direction vectors, $\left(\vec{u}_d\right)_{\text{tilt}}$ and $\left(\vec{u}_d\right)_{\text{roll}}$, were applied to the center of rotation shown in Figure 1b.

The momentum source term under the ship tilting and motion in Table 1, $\left(\vec{S}_{\text{G or L}}\right)_{\text{ship}}$, is expressed as follows

$$\left(\vec{S}_{\text{G}}\right)_{\text{ship}} = S'_{\text{G}x} \cdot \vec{i}' + S'_{\text{G}y} \cdot \vec{j}' + S'_{\text{G}z} \cdot \vec{k}'$$
$$\left(\vec{S}_{\text{L}}\right)_{\text{ship}} = S'_{\text{L}x} \cdot \vec{i}' + S'_{\text{L}y} \cdot \vec{j}' + S'_{\text{L}z} \cdot \vec{k}' \tag{4}$$

where $\vec{i}'$ and $\vec{j}'$ are the new direction vectors with a tilting angle of θ, as shown in Figure 3. The source terms in the new Cartesian coordinate ($\vec{S}'_{\text{G or L}}$) are described within the old coordinate ($\vec{i}$ and $\vec{j}$) by the vector decomposition. The z-direction does not change in the present ship tilting and motion. The source term in the gas phase ($\vec{S}'_{\text{G}}$) is expressed as

Table 1. Eulerian-Eulerian Porous Media CFD Model of Amine Absorber for MEA-CO_2 System

Equation Name	Equations	Eq. No.	Reference
Continuity equation	$\frac{\partial}{\partial}(\alpha_G\rho_G)=-\vec{\nabla}\cdot\left[\alpha_G\rho_G\left(\vec{u}_G-\vec{v}_{mesh}\right)\right]-r_{GL}$	T1	
	$\frac{\partial}{\partial}(\alpha_L\rho_L)=-\vec{\nabla}\cdot\left[\alpha_L\rho_L\left(\vec{u}_L-\vec{v}_{mesh}\right)\right]+r_{GL}$		
Momentum equation	$\rho_G\frac{\partial(\alpha_G\vec{u}_G)}{\partial t}=-\rho_G\vec{u}_G\cdot\vec{\nabla}[\alpha_G(\vec{u}_G-\vec{v}_{mesh})]-\vec{\nabla}P+\mu_G\vec{\nabla}\cdot\vec{\nabla}(\alpha_G(\vec{u}_G-\vec{v}_{mesh}))+\rho_G\alpha_G\vec{g}-\left(\vec{S}_G\right)_{ship}$	T2	
	$\rho_L\frac{\partial(\alpha_L\vec{u}_L)}{\partial t}=-\rho_L\vec{u}_L\cdot\vec{\nabla}[\alpha_L(\vec{u}_L-\vec{v}_{mesh})]-\vec{\nabla}P+\mu_L\vec{\nabla}\cdot\vec{\nabla}(\alpha_L(\vec{u}_L-\vec{v}_{mesh}))+\rho_L\alpha_L\vec{g}-\left(\vec{S}_L\right)_{ship}$		
	$\vec{S}'_G=\frac{\alpha_G}{\varepsilon}\vec{F}_{porous,G}+\varepsilon\vec{F}_{exch,GL}+\vec{F}_{disp,G}$	T3	Fourati et al.[13]
	$\vec{S}'_L=\frac{\alpha_L}{\varepsilon}\vec{F}_{porous,L}-\varepsilon\vec{F}_{exch,GL}+\vec{F}_{disp,L}$		
	$\vec{F}_{porous,G}=(1-f_e)\left(\frac{a\cdot E_1}{36}\cdot\frac{a_s^2}{\varepsilon}\mu_G+\frac{b\cdot E_2}{6}\cdot\frac{a_s\alpha_G\rho_G}{\varepsilon}\lvert\vec{u}_G\rvert\right)\vec{u}_G\equiv K_{GS}\vec{u}_G$	T4	Fourati et al.[13]
	$\vec{F}_{porous,L}=f_e\left(\frac{a\cdot E_1}{36}\cdot\frac{\varepsilon a_s^2}{\alpha_L^2}\mu_L+\frac{b\cdot E_2}{6}\cdot\frac{\varepsilon a_s}{\alpha_L}\rho_L\lvert\vec{u}_L\rvert\right)\vec{u}_L\equiv K_{LS}\vec{u}_L$		
	$\vec{F}_{exch,GL}=f_e\left(\frac{c\cdot E_1}{36}\cdot\frac{a_s^2}{\varepsilon\alpha_G}\mu_G+\frac{d\cdot E_2}{6}\cdot\frac{a_s}{\varepsilon}\rho_G\lvert\vec{u}_G-\vec{u}_L\rvert\right)\cdot(\vec{u}_G-\vec{u}_L)\equiv K_{IG}(\vec{u}_G-\vec{u}_L)$	T5	Fourati et al.[13]
	$\vec{F}_{disp,G}=\alpha_G K_{GS}\vec{u}_{D,G}+\varepsilon K_{IG}(\vec{u}_{D,G}-\vec{u}_{D,L})$	T6	Fourati et al.[13]; Lappalainen et al.[19]
	$\vec{F}_{disp,L}=\alpha_L K_{LS}\vec{u}_{D,L}-\varepsilon K_{IG}(\vec{u}_{D,G}-\vec{u}_{D,L})$		
	$\vec{u}_{D,G}=-f_{spread}\frac{\lvert\vec{u}_G/\alpha_G\rvert}{\alpha_G}\vec{\nabla}\alpha_G$		
	$\vec{u}_{D,L}=-f_{spread}\frac{\lvert\vec{u}_L\rvert}{\alpha_L}\vec{\nabla}\alpha_L$		
Mass equation	$\frac{\partial(\alpha_G\rho_{G,i})}{\partial t}=-(\vec{u}_G-\vec{v}_{mesh})\cdot\vec{\nabla}(\alpha_G\rho_{G,i})+D_{G,i}\nabla^2(\alpha_G\rho_{G,i})-r_{GL,i},\quad i=CO_2$	T7	Pham et al.[14]
	$\frac{\partial(\alpha_L\rho_{L,k})}{\partial t}=-(\vec{u}_L-\vec{v}_{mesh})\cdot\vec{\nabla}(\alpha_L\rho_{L,k})+D_{L,k}\nabla^2(\alpha_L\rho_{L,k})+r_{GL,i}+\alpha_L R_k,\quad k=\text{MEA, }CO_2\text{, ...}$		
	$r_{GL}=k_x a_e(\rho^*_{L,CO_2}-\rho_{L,CO_2})$	T8	Penttilä et al.[20]
	$\rho^*_{CO_2}=M_{w,CO_2}\frac{P_{CO_2}}{H_{CO_2-MEA}}$, where $H_{CO_2-MEA}=H_{N_2O-MEA}\frac{H_{CO_2-water}}{H_{N_2O-water}}$		
	$\frac{dC_{CO_2}}{dt}=-k_c C_{CO_2}C_{MEA}$, where $k_c=k_0e^{-E_a/RT}$, and $C_i=\frac{\rho_{L,i}}{M_{w,i}}$	T9	Hikita et al.[4]

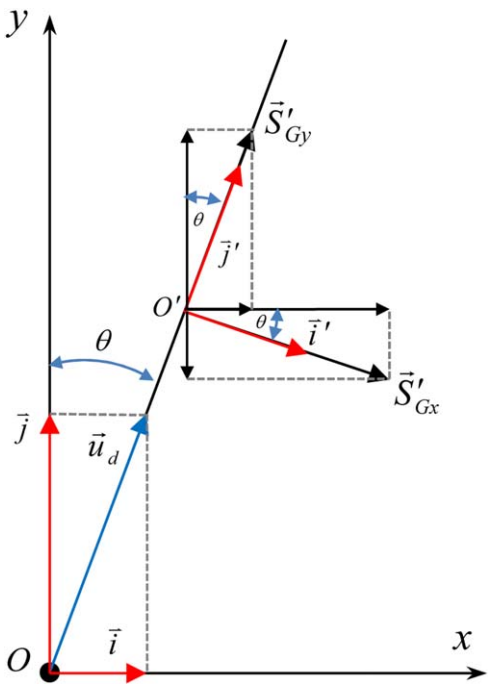

Figure 3. Unit direction vector ($\vec{u}_d$) and source term vectors ($\vec{S}'_{Gx}$ and $\vec{S}'_{Gy}$) in *x-y* Cartesian coordinate.

[Color figure can be viewed in the online issue, which is available at wileyonlinelibrary.com.]

$$S'_{Gx}\cdot\vec{i}' = |\vec{S}'_{Gx}|\cdot\cos\theta\cdot\vec{i} - |\vec{S}'_{Gx}|\cdot\sin\theta\cdot\vec{j}$$
$$S'_{Gy}\cdot\vec{j}' = |S'_{Gy}|\cdot\sin\theta\cdot\vec{i} + |S'_{Gy}|\cdot\cos\theta\cdot\vec{j} \quad (5)$$
$$S'_{Gz}\cdot\vec{k}' = S_{Gz}\cdot\vec{k}$$

Figure 3 illustrates the vector decomposition of $\vec{S}'_{Gx}$ and $\vec{S}'_{Gy}$. The source term vectors ($\vec{S}'_{G\,or\,L}$) are expressed in Eq. T3 of Table 1.

In this study, three tilting angles and motion amplitudes (1.5, 3.0, and 4.5°) were analyzed, and the motion period was set to 6 and 12 s. The static tilting angle of 4.5° is the most serious situation but is rare in reality. The ocean wave period usually varies between 4 and 15 s.[21] A severe wave condition with a period of 12 s was used for the south-east coast of Africa in this study.

Porous Media Eulerian CFD Model

A 3-D porous media CFD model was developed for the amine absorber. The fluid flow was assumed to be incompressible and isothermal. The gas and liquid phases were modeled by the Eulerian approach that treats the two phases flow as the interpenetrating continua. The porous resistance and liquid dispersion were considered to imitate hydrodynamics of the structured-packing in a macroscopic manner. The momentum and mass transfers between the two phases were taken into account and one chemical reaction occurred in the liquid phase.

Table 1 summarizes the porous media Eulerian CFD model in the gas and liquid phases. The voidage (ε) is defined as the gas and liquid volume fractions (α_G and α_L, respectively)

$$\varepsilon = \frac{V_G + V_L}{V} = \alpha_G + \alpha_L \quad (6)$$

where V_G is the gas volume, V_L is the liquid volume, and V includes V_G, V_L, and the solid volume of corrugated sheet metal. The continuity equation in Eq. T1 is served to calculate α_G and α_L. It is supposed that the voidage is uniform everywhere in the porous media zone.

The momentum equation is formulated on the basis of Fourati et al.[13] The modification factors (a, b, c, and d) of the Ergun coefficient in Eqs. T4 and T5 should be adjusted according to the packing type. The Ergun coefficients (E_1 and E_2) were set to 160 and 0.16, respectively, and the modification factors (a, b, c, and d) were found to be 1.9, 1.37, 0.17, and 1.16 for M500X.[14] The mass-transfer effect on the momentum equation in Eq. T2 was not considered, which may be small.

Wetting-area fraction (f_e)

The wetting-area fraction (f_e) in Eq. T4 is the ratio of the effective contacting area (a_e) between the gas and liquid phases to the specific surface area (a_s), which plays a crucial role in connecting hydrodynamics and mass transfer. As a_e cannot be directly captured in the porous media CFD, a function inspired from Tsai et al. (2011)[22] was used

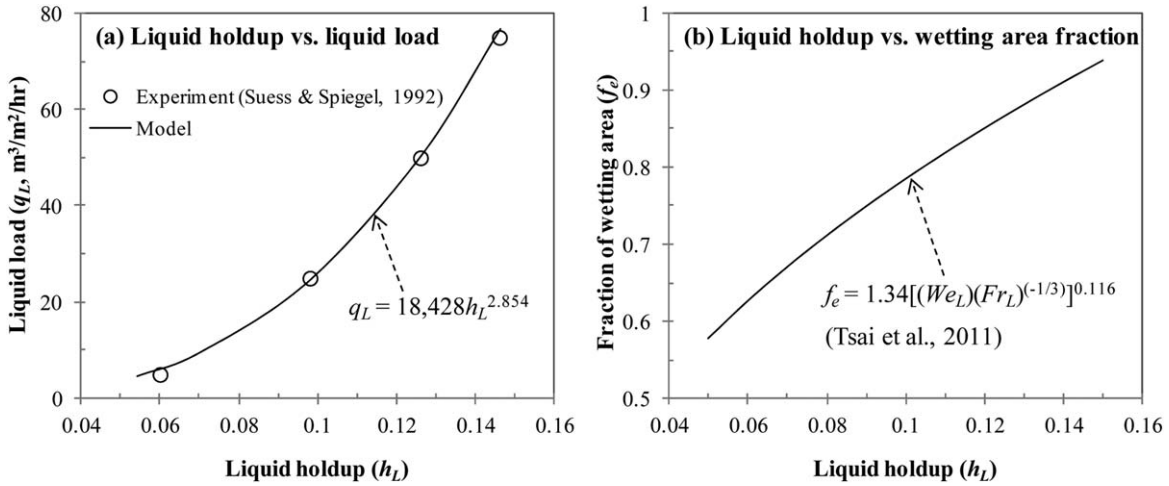

Figure 4. Fraction of wetting area (f_e) with respect to local liquid holdup (h_L).

Table 2. Boundary Condition (BC) of Amine Absorber

	Value
Bottom-side BC	Incompressible ideal gas inlet (back flow), liquid (pressure-outlet), gas load (natural gas) = 38.5 kmol/m^2/h, and gas mole composition: CH_4 = 0.85, CO_2 = 0.15.
Top-side BC	Gas (mass flow outlet)
Liquid distributor BC	Liquid (mass flow inlet), liquid load = 22.9 m^3/m^2/h, and liquid mass composition: MEA = 0.317, H_2O = 0.683.

$$f_e = \frac{a_e}{a_s} = 1.34\left[\frac{\rho_L}{\sigma} g^{1/3}\left(\frac{Q}{L_p}\right)^{4/3}\right]^{0.116} \quad (7)$$

$$Q = 5.1189 A h_L^{2.854}$$

where ρ_L [= 998 kg/m^3] is the liquid density, σ [= 0.072 N/m] is the surface tension of MEA solution, g [= 9.81 m/s^2] is the gravity acceleration, Q [m^3/s] is the liquid flow rate, L_p [= 4.0 6m] means the wetted perimeter, A [= 0.00785 m^2] is the cross-sectional area of column, and h_L is the liquid holdup. The function of q_L (= 3600Q/A) and h_L was fitted from an air-water experiment of Suess and Spiegel (1992),[23] as shown in Figure 4a. Their experiment was performed for M500Y in $5 \le q_L \le 75$ m^3/m^2/h. Figure 4b shows the fraction of wetting area (f_e) with respect to the liquid holdup (h_L). Fortunately, h_L of the amine absorber varied from 0.085 to 0.093 (see Section Results and Discussion), which was calculated from this CFD simulation by a local value of the liquid volume fraction (α_L) over an interesting volume

$$h_L = \frac{\sum_i \alpha_{L,i} \Delta V_i}{\sum_i \Delta V_i} \quad (8)$$

where ΔV is the cell volume in the computational domain. It is expected that the empirical equation (7) is valid in our simulation range.

Liquid spreading factor (f_{spread})

The liquid spread inside structured packing is modeled by Eq. T6,[13,19] where the liquid spreading factor (f_e) was estimated from a convection and diffusion equation of liquid load (q_L).[13] f_{spread} = 3.7 and 7.4 mm were suggested for M250X. In the present simulation, f_{spread} = 7.4 mm was used for M500X as a default value.

Mass transfer and chemical reaction

It was assumed that there are two species such as CH_4 and CO_2 in the gas phase. It was also supposed that MEA and

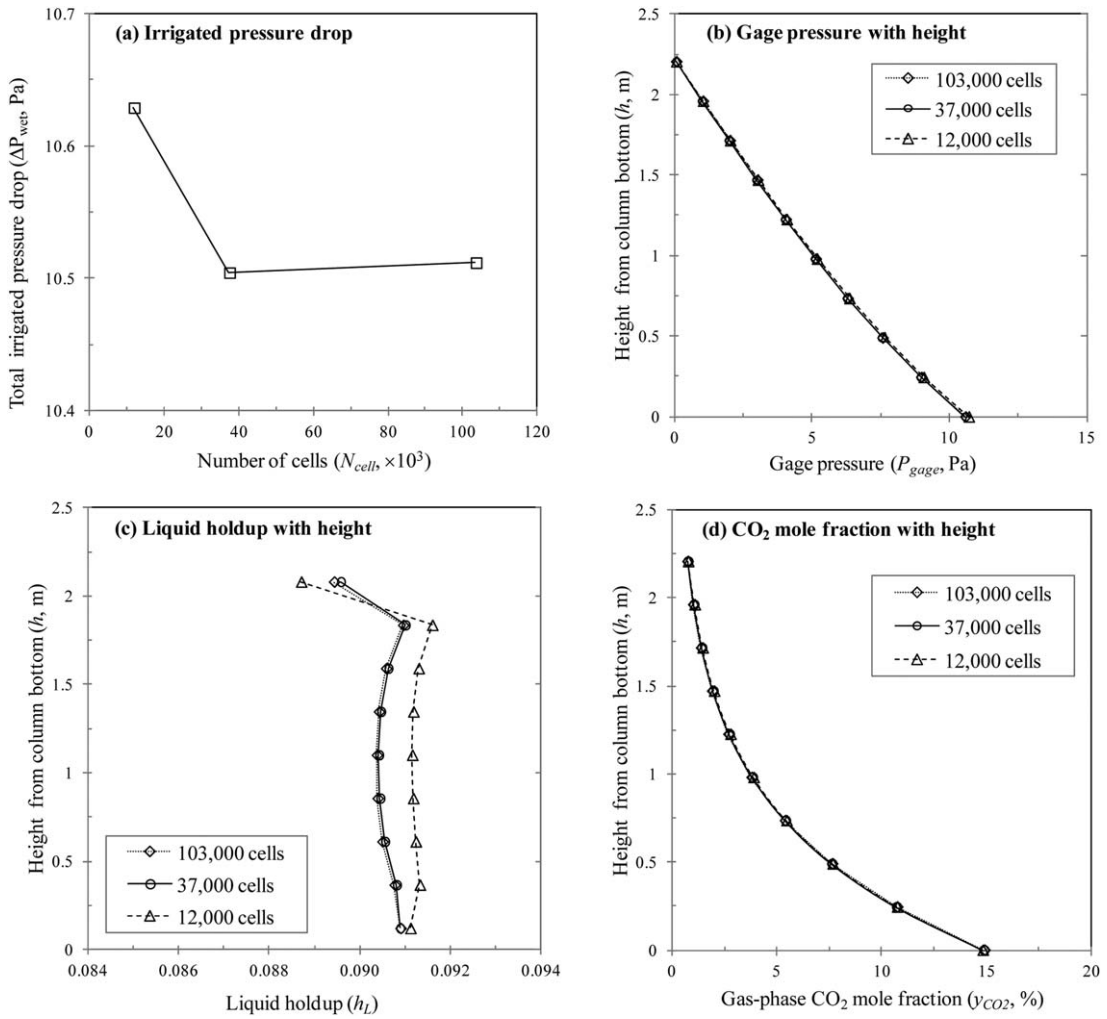

Figure 5. Mesh independent test on coarse, medium, and fine meshes at 3° static tilting.

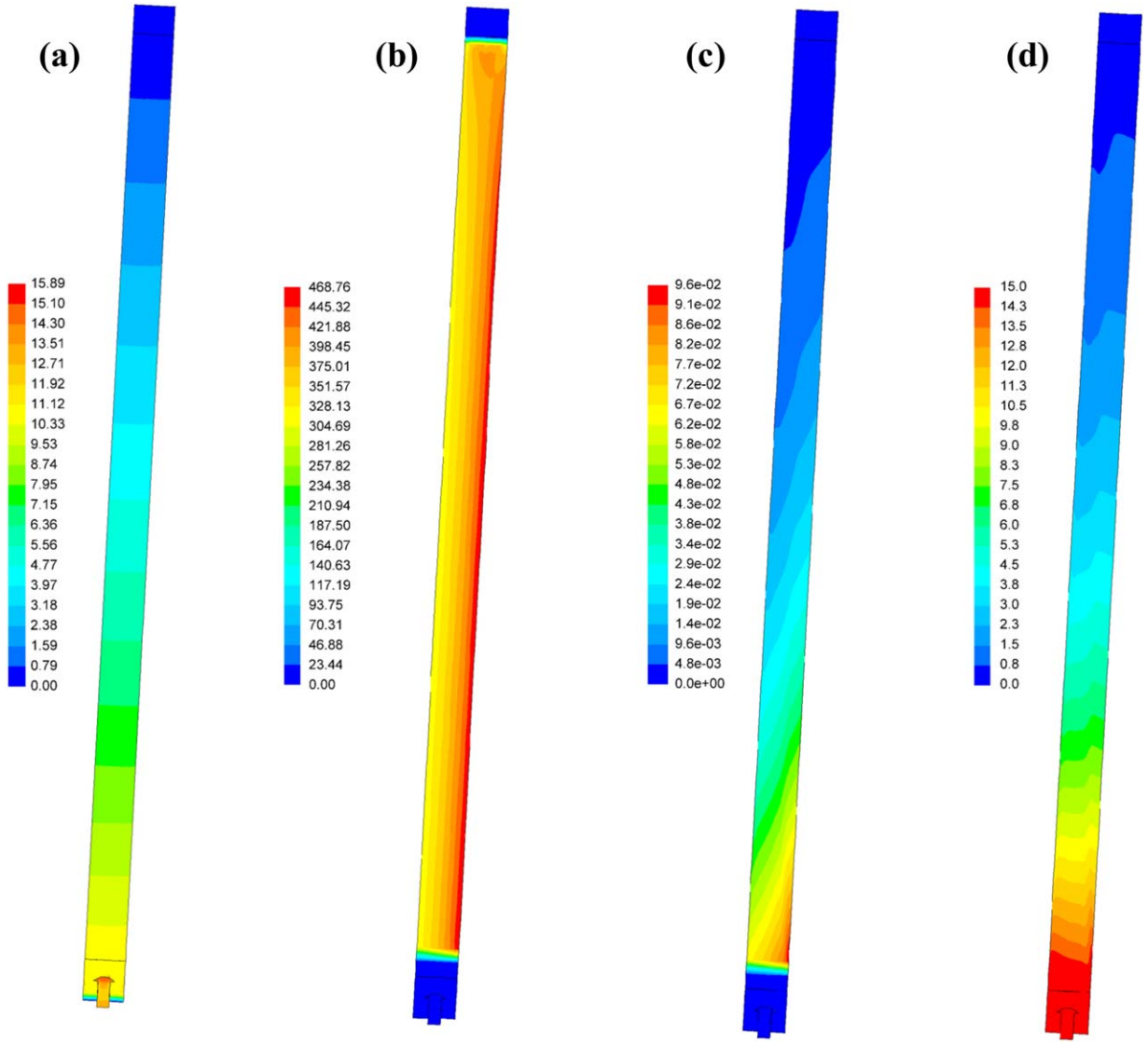

Figure 6. Effect of 3° static tilting on (a) gage pressure (P_{gage}, Pa), (b) effective interfacial area (a_e, m^2/m^3), (c) mass-transfer rate of CO_2 (r_{CO_2}, $kg/m^3/s$), and (d) CO_2 mole fraction in the gas phase (y_{CO_2}, %).

[Color figure can be viewed in the online issue, which is available at wileyonlinelibrary.com.]

other species in the liquid phase do not vaporize into the gas phase. Even though the reactions during the absorption of CO_2 into the aqueous amine solution are complex, just one chemical reaction is considered in this study for the CO_2-MEA system.[4] Assuming that mass transfer between the gas and liquid phases occurs for only CO_2, the mass conservation equation is expressed in Eqs. T7–T9.

As most of the overall mass-transfer resistance comes from the liquid-side resistance in the CO_2-amine system,[24,25] the mass-transfer rate (r_{GL}) is expressed as the liquid-film mass-transfer coefficient (k_x) and the driving force of liquid concentrations in Eq. T8. Here, k_x [= 0.00104 m/s] represents a lumped value including the liquid film resistance and the enhancement by the chemical reaction.[14] The equilibrium concentration (ρ^*_{L,CO_2}) is determined by Henry's law. The Henry's constant used in this study was $H_{CO_2\text{-MEA}} = 3690$ Pa m^3/mol at 304 K.[20]

One simple chemical reaction rate between CO_2 and MEA proposed by Hikita et al.[4] was applied with $k_0 = 5.928 \times 10^4$ m^3/kmol/s and $E_a = 4.274 \times 10^3$ kcal/kmol. The diffusivities of natural gas and MEA solution were assumed to be constant at $D_G = 2.8 \times 10^{-7}$, and $D_L = 2.88 \times 10^{-9}$ m^2/s, respectively.

Operating and boundary conditions

The amine absorber was operated at 304 K and 1 atm. Gas and liquid inlet boundary conditions (inlet BC) were taken from experimental conditions of Aroonwilas et al.[16] The outlet boundary condition (outlet BC) of gas was set to the mass flow outlet, while that of liquid was the pressure outlet. Table 2 indicates the boundary conditions.

Results and Discussion

The continuity equation, momentum, and mass conservation equations were solved by using ANSYS Fluent (ANSYS). Three user-defined functions (UDFs) were supplied to the conventional CFD model: (1) three additional momentum terms ($\vec{F}_{porous}$, $\vec{F}_{exch,GL}$, and $\vec{F}_{disp}$) in Eqs. T4–T6 for the porous media zone, (2) mass-transfer rate (r_{GL}) and chemical reaction rates (R_k) in Eqs. T8 and T9, and (3) ship tilting and motion in

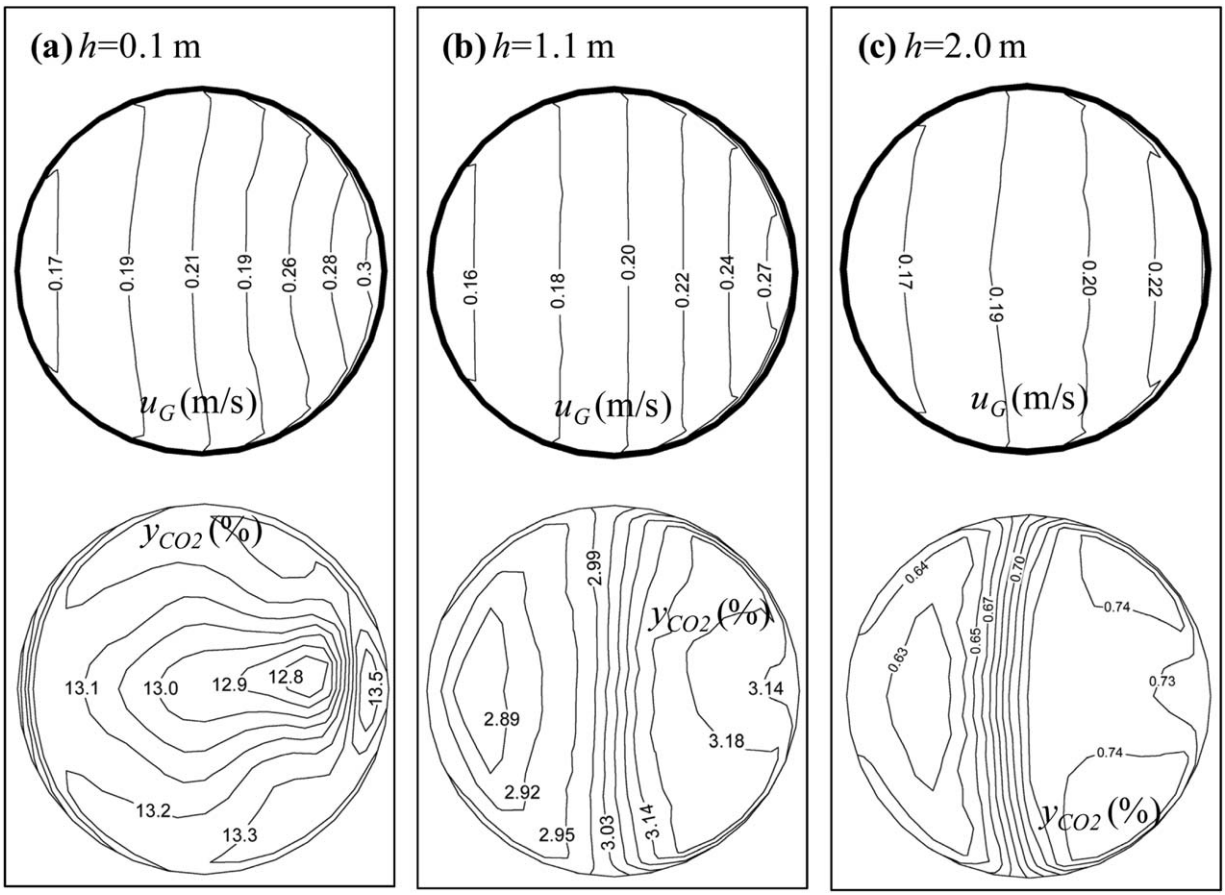

Figure 7. Contours of gas velocity (u_G) and CO_2 mole fraction (y_{CO_2}) over the cross-sectional area along the column height.

Eqs. 1–5. The phase coupled SIMPLE method was chosen for pressure–velocity coupling. The second-order upwind scheme was used for the spatial discretization of the momentum and mass equations. The multiphase Eulerian model was calculated by the unsteady-state, sequential (or pressure-based segregated), and implicit solver. The maximum iteration number was 100 at each time step, and the convergence tolerance was 1×10^{-3}.

Mesh independent test

The mesh independent test was performed on the coarse, medium, and fine meshes for the porous zone under the 3° static tilting condition. The effect of the mesh number was examined on the total wet pressure drop (ΔP_{wet}), and gage pressure (P_{gage}), liquid holdup (h_L), and CO_2 mole fraction (y_{CO_2}) along the column height, as shown in Figure 5.

As the structured-packing was regarded as a homogeneous porous material with viscous and inertial momentum loss, the effect of the mesh number was not significant on ΔP_{wet}, P_{gage}, and y_{CO_2}. The difference of ΔP_{wet} on the coarse and fine grids is only 0.12 Pa (= 1.1%) for the column height of 2.2 m, as seen in Figure 5a. In Figures 5b, d, it is more clear that the mesh number barely affect P_{gage} and y_{CO_2}. However, some discrepancy of h_L is observed in Figure 5c according to the mesh resolution. The average liquid holdup of the coarse mesh shows a relative difference of 0.6% from those of the medium and fine meshes. In fact, the porous media approach is not susceptible to the number of cells. The medium mesh was selected from this mesh independence test as a compromise between accuracy and computational efficiency.

Effect of static tilting

The effect of 3° static tilting on P_{gage}, a_e, r_{CO_2}, and y_{CO_2} is illustrated in Figure 6. The liquid spreading factor (f_{spread}) was set to 7.4 mm.[13] P_{gage} is relatively symmetric from the center line of the column (see Figure 6a), which may increase slightly due to the local premature flooding in the tilting case.[10] The deviation of the liquid distribution in the radial direction is clearly observed in Figure 6b. The effective interfacial area (a_e) is higher on the tilting side and the mass-transfer rate (r_{CO_2}) is higher (see Figure 6c). Figure 6d displays an asymmetric behavior of y_{CO_2}. The CO_2 concentration is lower on the tilting side than the other side at the bottom of the column where the mass-transfer rate is dominant (see also Figure 6c). However, the CO_2 concentration crosses over from one fourth of the column height. y_{CO_2} of the tilting side is higher at the top, and the maximum and minimum concentrations appear inside the column.

Figure 7 illustrates the contours of gas velocity (u_G, m/s) and CO_2 mole fraction (y_{CO_2}, %) over the cross-sectional area at three different heights: bottom, middle, and top of the packing zone. The gas velocity is biased on the tilting side. The extent of the velocity bias slightly decreases as the height increases. The highest y_{CO_2} is observed near the wall on the tilting side (or right-hand side), which may be due to the highest gas velocity on this side. The difference of CO_2 concentrations over the cross-sectional area is not high (0.1–0.7%). However, the minimum y_{CO_2} changes from the right to the left side along the column height, as mentioned above. This behavior would be confirmed for the real structured-packing

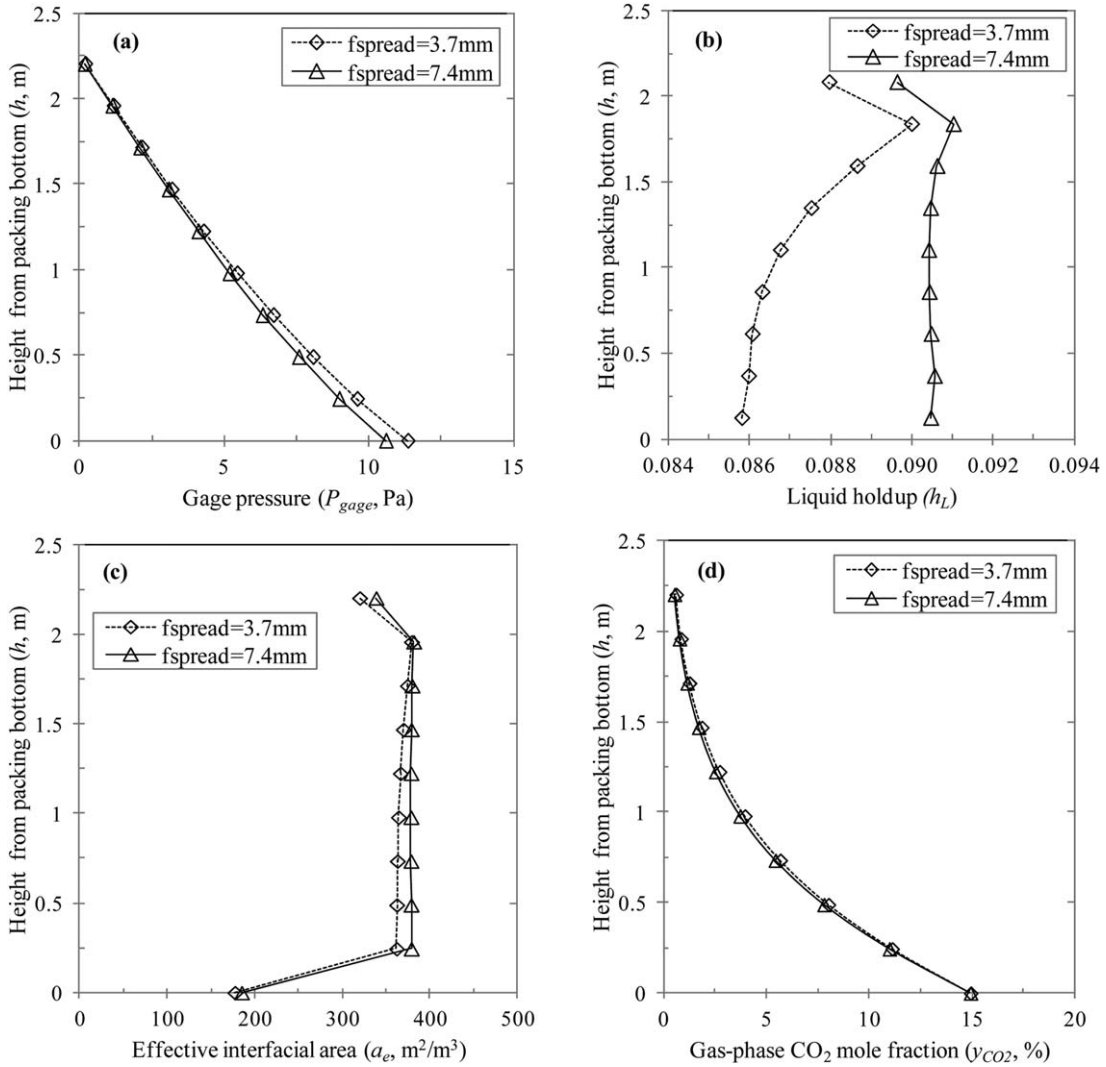

Figure 8. Effect of liquid spreading factor (f_{spread}) on (a) gauge pressure (P_{gage}, Pa), (b) liquid holdup (h_L), (c) effective interfacial area (a_e, m^2/m^3), and (d) CO_2 mole fraction in the gas phase (y_{CO_2}, %) at 3° static tilting.

with a corrugated, perforated, and microscopic-grooved metal sheet.

Under the 3° tilting condition, the effect of f_{spread} on P_{gage}, h_L, a_e, and y_{CO_2} is shown in Figure 8. The higher f_{spread} leads to the higher h_L, a_e, but the lower y_{CO_2}. However, the pressure drop of $f_{spread} = 7.4$ mm is slightly lower than that of $f_{spread} = 3.7$ mm, because a localized liquid spread at $f_{spread} = 3.7$ mm increases the pressure drop.

Figure 9 shows the effect of the tilting angle on P_{gage}, h_L, a_e, and y_{CO_2}. The tilting of 0° means the vertical standing. The average h_L of vertical standing is 9.2%, which coincides with the experimental value of M500X.[10] As the tilting angle increases, the pressure drop slightly increases, and h_L and a_e, decrease. As the CO_2 removal efficiency cannot be apparently distinguished for the four tilting angles in Figure 9d, a definite comparison is followed below.

Comparison of vertical standing, static tilting, and rolling motion

At the beginning of the simulation, gas and liquid were injected into the packed column which was initially empty. After a wetting period of about 35 s, the mass transfer and chemical reaction started, and it took about 15 s to reach a stable state. Thus, an operating time of about 50 s was required to obtain a stable solution under the vertical standing condition. Once the stable state is reached, the dynamic motion starts and a cyclic steady state is observed after 20 s. A cyclic steady state of a_e is illustrated with the flow time (t) in Figure 10. The column performance values under the rolling motion were obtained from the average of five flow times for one period ($T = 12$ s).

Figure 11 compares P_{gage}, h_L, a_e, and y_{CO_2} of three cases: vertical standing, 3° static tilting, and angular motion of 3° amplitude at 6 and 12 s periods. Experimental concentrations along the height measured for CO_2-MEA system with M500X[16] are shown in Figure 11d. The results of the porous media CFD model agree well with the experimental CO_2 removal. The tilting and motion increase the pressure drop a little (see Figure 11a). The static tilting decreases more the liquid holdup and effective interfacial area more than the rolling motion (see Figures 11b, c), which was also identified by experiment.[11] However, the CO_2 removal efficiency is almost the same for the three cases, because such a difference of a_e is not significant for the CO_2 removal in this amine absorber (see Figure 11d).

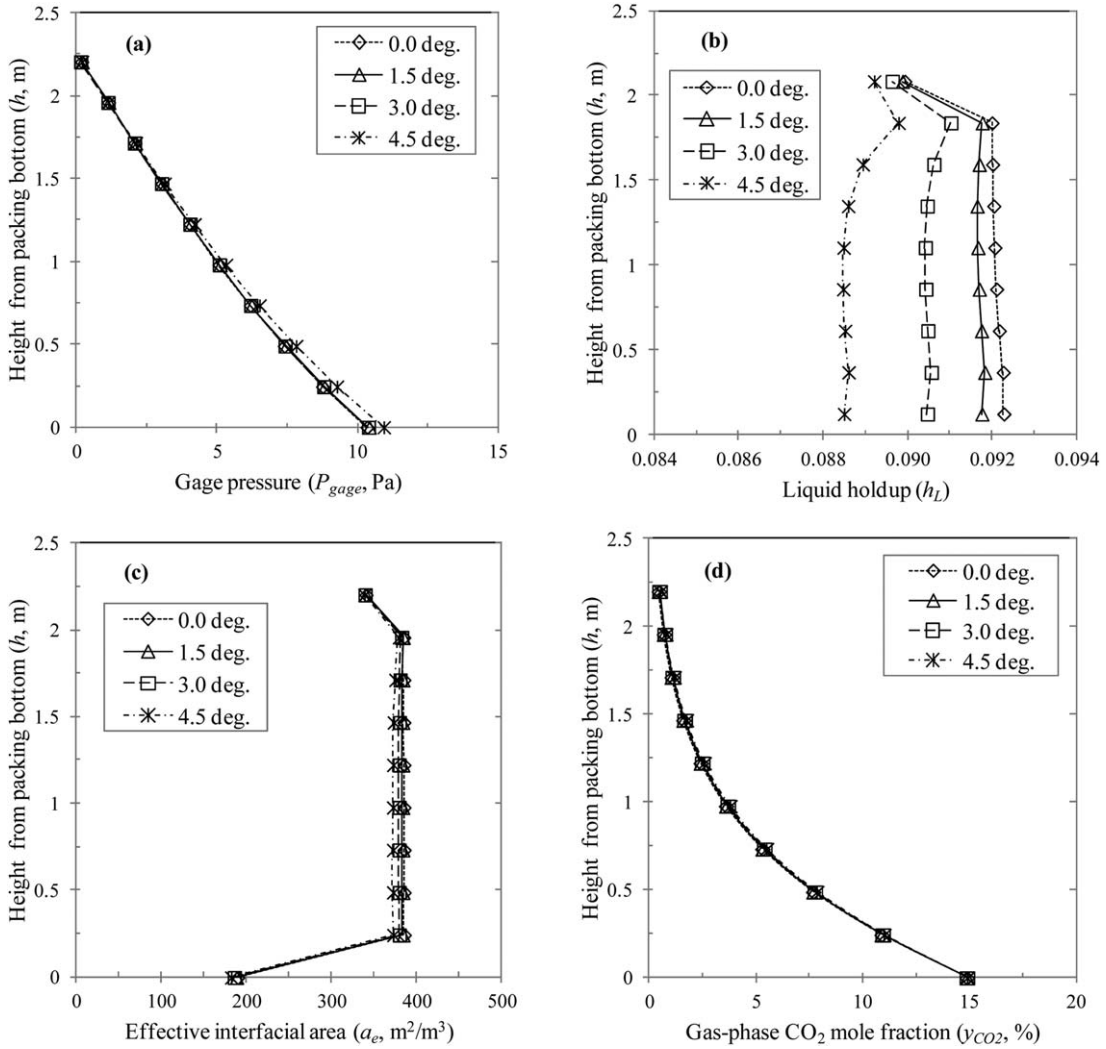

Figure 9. Effect of tilting angle on (a) gauge pressure (P_{gage}, Pa), (b) liquid holdup (h_L), (c) effective interfacial area (a_e, m^2/m^3), and (d) CO_2 mole fraction in the gas phase (y_{CO_2}, %).

The effect of the rolling motion on the amine absorber performance is less serious than that of the static tilting, as mentioned earlier. Figure 12 shows the effect of the amplitude of the rolling motion at the same period. The fluctuation of its liquid holdup along the column height is greater than that of the static tilting. However, the impact of the tilting angle (or amplitude) on h_L is smaller in the rolling motion than in the static tilting.

The liquid velocity calculated from the CFD simulation was $u_L = 0.19$ m/s. The residence time of liquid was about 11.5 s which was almost the same value as the rolling period. The smaller the rolling period at the same amplitude, the higher the liquid holdup, as shown in Figure 11b. The arc length is proportional to the absorber height and the amplitude ($l = h\theta$) in the rolling motion. If the absorber height is long, the tangential velocity increases along the column height and the effect of the ship motion on the liquid holdup becomes severe.

Uniformity index and CO_2 removal efficiency

Two uniformity indexes (UI) that represent liquid mal-distribution are defined as follows

$$\mathrm{UI}_v = 1 - \frac{\sum_{i=1}^{n} \left(|u_{\mathrm{L},i} - \bar{u}_\mathrm{L}| A_i \right)}{2\bar{u}_\mathrm{L} \sum_{i=1}^{n} A_i}$$
$$\mathrm{UI}_h = 1 - \frac{\sum_{i=1}^{n} \left(|h_{\mathrm{L},i} - \bar{h}_\mathrm{L}| A_i \right)}{2\bar{h}_\mathrm{L} \sum_{i=1}^{n} A_i} \quad (9)$$

where UI_v and UI_h are the UI of liquid velocity and holdup, respectively. i is the facet index of a surface with n facets, A_i is the area of i-facet, and $\bar{u}_\mathrm{L}$ and $\bar{h}_\mathrm{L}$ are the average value of the liquid velocity and holdup, respectively. Table 3 compares UI_v and UI_h of the eight runs for the three cases. The uniformity indexes were calculated in the cross-sectional area at $h = 0.1$ m. The UI_v and UI_h shows almost the same trend. It was found that a deterioration of around 10% in the liquid distribution occurs for the 3° static tilting and the rolling motion with 4.5° at 12 s.

The CO_2 removal efficiency (η, %) is defined as

$$\eta = 100 \times \frac{y_{\mathrm{CO_2,in}} - y_{\mathrm{CO_2,out}}}{y_{\mathrm{CO_2,in}}} \quad (10)$$

In Table 4, η is compared for the eight runs. The static tilting of 4.5° as the most severe case decreases the efficiency by 0.4% and the rolling motion with 4.5° and 12 s by 0.1%. It is

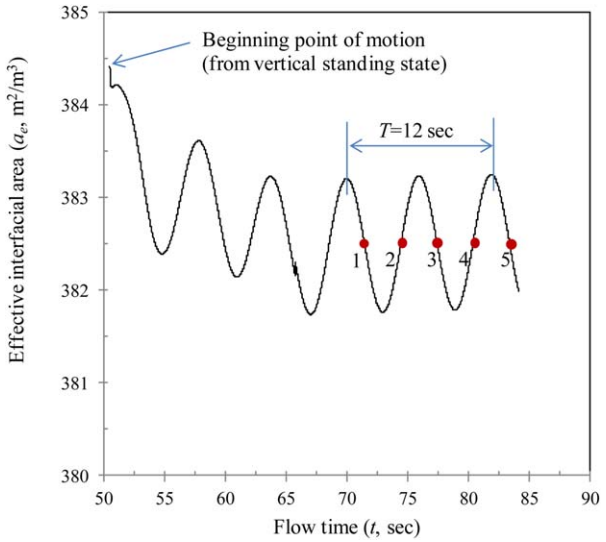

Figure 10. Cyclic steady state of effective interfacial area (a_e) under rolling motion.

[Color figure can be viewed in the online issue, which is available at wileyonlinelibrary.com.]

noted that the difference of η is small while that of UI_h is relatively large. It is attributed from the fact that the effective interfacial area does not change much by the tilting and motion and the chemical reaction rate is relatively high in this CO_2-MEA system.

Conclusions

The 3-D geometry of an amine absorber packed with nine elements of Mellapak 500.X (M500X) was built to investigate the effect of ship tilting and motion on the amine absorber performance. The amine absorber was operated to remove 15 mol % CO_2 contained in natural gas using MEA as an absorbent. To represent the structured-packing by the porous media CFD model, the porous resistance force, the gas-liquid momentum exchange, and the liquid dispersion force were added into the momentum conservation equation. The mass conservation equation included the mass transfer between the gas and liquid phases, and one chemical reaction in the liquid phase. The two phases were modeled as a continuum using the Eulerian approach. The gas-liquid Eulerian porous media CFD model was calculated by a finite volume-based solver, ANSYS Fluent.

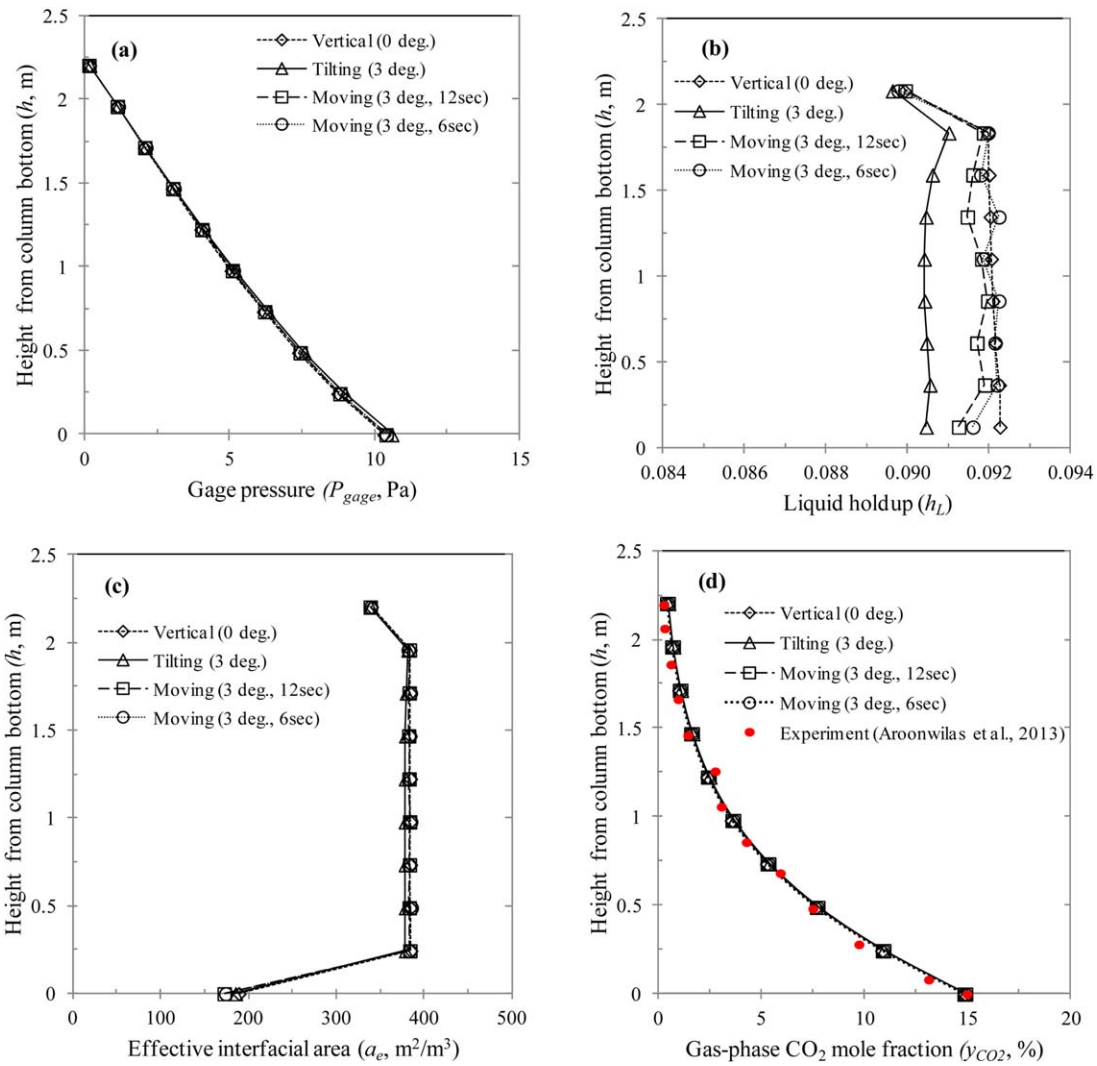

Figure 11. Effect of ship tilting and motion on (a) gauge pressure (P_{gage}, Pa), (b) liquid holdup (h_L), (c) effective interfacial area (a_e, m^2/m^3), and (d) CO_2 mole fraction in the gas phase (y_{CO_2}, %).

[Color figure can be viewed in the online issue, which is available at wileyonlinelibrary.com.]

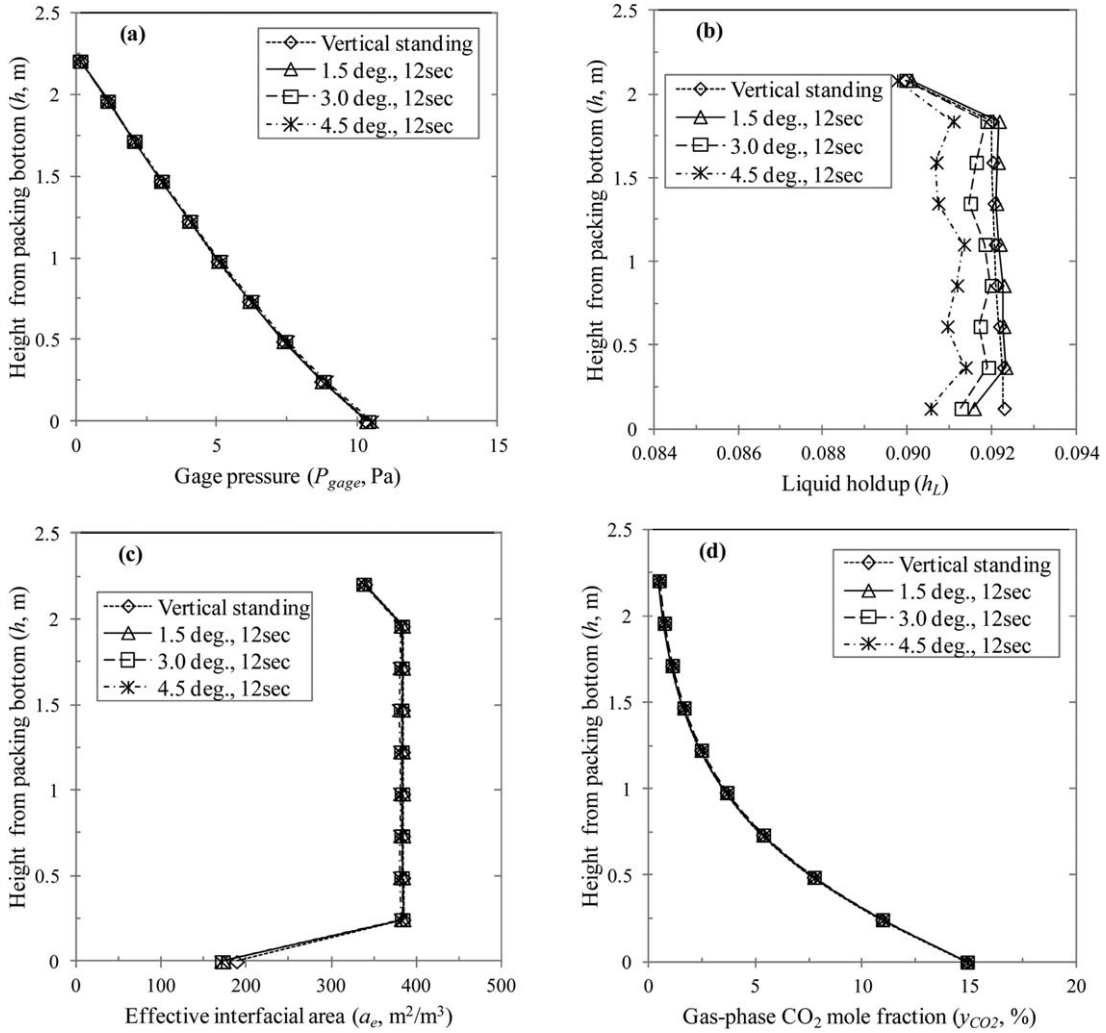

Figure 12. Effect of rolling motion amplitude on (a) gauge pressure (P_{gage}, Pa), (b) liquid holdup (h_L), (c) effective interfacial area (a_e, m^2/m^3), and (d) CO_2 mole fraction in the gas phase (y_{CO_2}, %).

Table 3. Comparison of Uniformity Index of Liquid Holdup

Case	Vertical Standing	Static Tilting			Rolling Motion			
Run number	1	2	3	4	5	6	7	8
Angle (θ, °)	0	1.5	3.0	4.5	1.5	3.0	4.5	3.0
Period (T, s)	–	–	–	–	12	12	12	6
UI_v	0.999	0.950	0.901	0.854	0.976	0.954	0.930	0.968
UI_h	0.999	0.951	0.903	0.855	0.975	0.953	0.930	0.962

The coarse (11,900 cells), medium (37,400 cells), and fine (103,500 cells) meshes were constructed for the mesh independent test. The number of cells barely affected the pressure drop and CO_2 removal efficiency. However, the liquid holdup of the coarse mesh showed a significant difference from those of the medium and fine meshes. The medium mesh was selected among the three meshes for computational efficiency. The effective interfacial area between gas and liquid was estimated by an empirical equation as a function of the liquid holdup. The modification factors of the Ergun coefficients (a, b, c, and d) were adjusted for M500X, compared with experimental data.

Table 4. Comparison of CO_2 Removal Efficiency with MEA Absorbent

Case	Vertical Standing	Static Tilting			Rolling Motion			
Run number	1	2	3	4	5	6	7	8
Angle (θ,°)	0	1.5	3.0	4.5	1.5	3.0	4.5	3.0
Period (T, s)	–	–	–	–	12	12	12	6
CO_2 removal efficiency (η, %)	96.84	96.80	96.63	96.42	96.82	96.77	96.71	96.81

As the static tilting angle increases, the liquid holdup and effective interfacial area decreases and the CO_2 removal efficiency is lowered. The effect of the static tilting on the liquid holdup is more severe than that of the rolling motion, when the angle or amplitude is the same. The uniformity index of the liquid holdup deteriorates by 10% for the 3° static tilting, and the angular motion with a 3° amplitude at a 12 s period, respectively. The CO_2 removal efficiency decreases by 0.4% for the 4.5° static tilting, and by 0.1% for the rolling motion with a 4.5° amplitude at a 12 s period.

In this study, the effect of the ship tilting and motion on the amine absorber without internals such as collectors and redistributors was examined in an isothermal, isotropic, and homogeneous porous media, neglecting the temperature difference and the complex directional-properties of structured-packing column. The relationship between the orientation of packing elements and the tilting direction was ignored. Thus, some discrepancy from the real system is inevitable. However, a simple and efficient CFD model was proposed for the first time in the open literature to estimate the effect of the ship tilting and motion.

Acknowledgments

This research was supported by a grant from the Program of KAIA funded by the Ministry of Land, Infrastructure and Transport of the Korean government (08 GASPLANT F02). The authors appreciate the editing contribution of Patrick Bresnahan.

Notation

a = modification factor of Ergun equation
a_e = effective interfacial area, m^2/m^3
a_s = specific surface area of structured-packing, m^2/m^3
b = modification factor of Ergun equation
c = modification factor of Ergun equation
C_i = molar concentration of species i in liquid phase, $kmol/m^3$
d = modification factor of Ergun equation
D = diffusivity coefficient, m^2/s
E_1, E_2 = Ergun coefficients
E_a = activation energy, cal/gmol
$\vec{F}_{disp}$ = liquid dispersion force, N/m^3
f_e = fraction of wetting area
$\vec{F}_{exch}$ = momentum exchange force, N/m^3
$\vec{F}_{porous}$ = porous resistance force, N/m^3
f_{spread} = spread factor, m
g = gravitational acceleration, m/s^2
h = column height, m
h_L = liquid holdup, m^3/m^3
H = Henry's constant, Pa m^3/mol
k_0 = pre-exponential factor, $m^3/kmol/s$
k_c = chemical reaction rate coefficient, $m^3/kmol/s$
K_{GS} = gas-solid drag coefficient, $kg/m^3/s$
K_{IG} = momentum exchange coefficient at the gas-liquid interface, $kg/m^3/s$
K_{LS} = liquid-solid drag coefficient, $kg/m^3/s$
k_x = liquid-side mass-transfer coefficient, m/s
M_w = molecular weight, kg/kmol
P = pressure, atm
q_G = gas load, $kmol/m^2/h$
q_L = liquid load, $m^3/m^2/h$
$\vec{r}$ = position vector, m
r_{GL} = mass-transfer rate between gas and liquid, $kg/m^3/s$
R_i = chemical reaction rate of species i, $kg/m^3/s$
S = momentum source term, N/m^3
t = time, s
T = period, s
$\vec{u}$ = interstitial volume-average velocity, m/s
V = volume, m^3
y_i = gas mole fraction of species i

Greek symbols

α_G = volume fraction of gas phase
α_L = volume fraction of liquid phase
ε = packing void fraction (porosity)
θ = corrugation angle, °
μ = viscosity, kg/m/s
ρ = mass concentration or density, kg/m^3
$\vec{\omega}$ = angular velocity, s^{-1}

Subscripts

D = drift
G = gas phase
L = liquid phase

Literature Cited

1. Zhuang Q, Pomalis R, Zheng L, Clements B. Ammonia-based carbon dioxide capture technology: issues and solutions. *Energy Procedia*. 2011;4:1459–1470.
2. Kwak N-S, Lee JH, Lee IY, Jang KR, Shim J-G. A study of the CO_2 capture pilot plant by amine absorption. *Energy*. 2012;47(1): 41–46.
3. Mandal BP, Bandyopadhyay SS. Simultaneous absorption of carbon dioxide and hydrogen sulfide into aqueous blends of 2-amino-2-methyl-1-propanol and diethanolamine. *Chem Eng Sci*. 2005;60(22): 6438–6451.
4. Hikita H, Asai S, Ishikawa H, Honda M. The kinetics of reactions of carbon dioxide with monoethanolamine, diethanolamine and triethanolamine by a rapid mixing method. *Chem Eng J*. 1977;13(1):7–12.
5. Aroonwilas A, Tontiwachwuthikul P, Chakma A. Effects of operating and design parameters on CO_2 absorption in columns with structured packings. *Sep Purif Technol*. 2001;24(3):403–411.
6. Beugre D, Calvo S, Crine M, Toye D, Marchot P. Gas flow simulations in a structured packing by lattice Boltzmann method. *Chem Eng Sci*. 2011;66(17):3742–3752.
7. Owens SA, Perkins MR, Eldridge RB, Schulz KW, Ketcham RA. Computational fluid dynamics simulation of structured packing. *Ind Eng Chem Res*. 2013;52(5):2032–2045.
8. Sun B, He L, Liu BT, Gu F, Liu CJ. A new multi-scale model based on CFD and macroscopic calculation for corrugated structured packing column. *AlChE J*. 2013;59(8):3119–3130.
9. Duss M, Roza M. Columns subject to motion: maldistribution sensitivity and susceptibility. In *10th International Conference on Distillation & Absorption*. Friedrichshafen, Germany: Dechema, September 14–17, 2014:211–217.
10. Spiegel L, Duss M. Chapter 4 - Structured packings. In: Olujić AG, editor. *Distillation*. Boston: Academic Press, 2014:145–181.
11. White V, Kalbassi MA, Waldie B, Wilson J, Inventors. Structured Packing and Use Thereof. US Patent 7,673,857. 2010.
12. Mohamed Ali A, Jansens PJ, Olujić Ž. Experimental characterization and computational fluid dynamics simulation of gas distribution performance of liquid (re)distributors and collectors in packed columns. *Chem Eng Res Des*. 2003;81(1):108–115.
13. Fourati M, Roig V, Raynal L. Liquid dispersion in packed columns: experiments and numerical modeling. *Chem Eng Sci*. 2013;100:266–278.
14. Pham DA, Lim Y-I, Jee H, Ahn E, Jung Y. Porous media Eulerian computational fluid dynamics (CFD) model of amine absorber with structured-packing for CO_2 removal. *Chem Eng Sci*. 2015;132:259–270.
15. Raynal L, Royon-Lebeaud A. A multi-scale approach for CFD calculations of gas–liquid flow within large size column equipped with structured packing. *Chem Eng Sci*. 2007;62(24):7196–7204.
16. Aroonwilas A, Chakma A, Tontiwachwuthikul P, Veawab A. Mathematical modelling of mass-transfer and hydrodynamics in CO_2 absorbers packed with structured packings. *Chem Eng Sci*. 2003; 58(17):4037–4053.
17. Aroonwilas A, Tontiwachwuthikul P. Mechanistic model for prediction of structured packing mass transfer performance in CO_2 absorption with chemical reactions. *Chem Eng Sci*. 2000;55(18):3651–3663.
18. McCabe WL, Smith J, Harriott P. *Unit Operations of Chemical Engineering*, 7th ed. New York: McGraw-Hill, 2005.
19. Lappalainen K, Manninen M, Alopaeus V. CFD modeling of radial spreading of flow in trickle-bed reactors due to mechanical and capillary dispersion. *Chem Eng Sci*. 2009;64(2):207–218.

20. Penttilä A, Dell'Era C, Uusi-Kyyny P, Alopaeus V. The Henry's law constant of N_2O and CO_2 in aqueous binary and ternary amine solutions (MEA, DEA, DIPA, MDEA, and AMP). *Fluid Phase Equilib*. 2011;311:59–66.
21. WMO. *Guide to Wave Analysis and Forecasting*. *WMO-No. 702*. Geneva, Switzerland: World Meteorological Organization, 1998.
22. Tsai RE, Seibert AF, Eldridge RB, Rochelle GT. A dimensionless model for predicting the mass-transfer area of structured packing. *AIChE J*. 2011;57(5):1173–1184.
23. Suess P, Spiegel L. Hold-up of mellapak structured packings. *Chem Eng Process*. 1992;31(2):119–124.
24. Hamborg ES, Versteeg GF. Absorption and desorption mass transfer rates in chemically enhanced reactive systems. Part II: reverse kinetic rate parameters. *Chem Eng J*. 2012;198–199:561–570.
25. Tunnat A, Behr P, Görner K. Desorption kinetics of CO_2 from water and aqueous amine solutions. *Energy Procedia*. 2014;51:197–206.

Manuscript received Apr. 17, 2015, and revision received June 10, 2015.